

Blackening of metals using femtosecond fiber laser

Huan Huang,* Lih-Mei Yang, Shuang Bai, and Jian Liu

PolarOnyx, Inc. 2526 Qume Drive, Suite 17 & 18, San Jose, California 94538, USA

*Corresponding author: h Huang@polaronyx.com

Received 2 October 2014; revised 25 November 2014; accepted 28 November 2014;
posted 1 December 2014 (Doc. ID 224015); published 9 January 2015

This study presents an unprecedented high throughput processing for super-blackening and superhydrophobic/hydrophilic surface on both planar and nonplanar metals surfaces. By using a high pulse repetition rate femtosecond (fs) fiber laser, a light trapping microstructure and nanostructure is generated to absorb light from UV, visible to long-wave infrared spectral region. Different types of surface structures are produced with varying laser scanning conditions (scanning speed and pitch). The modified surface morphologies are characterized using scanning electron microscope and the blackening effect is investigated through spectral measurements. Spectral measurements show that the reflectance of the processed materials decreases sharply in a wide wavelength range and the decrease occurs at different rates for different scanning pitches and speeds. Above 98% absorption over the entire visible wavelength region and above 95% absorption over the near-infrared, middle-wave infrared and long-wave infrared regions range has been demonstrated for the surface structures, and the absorption for specific wavelengths can go above 99%. Furthermore, the processing efficiency of this fs fiber laser blackening technique is 1 order of magnitude higher than that of solid-state fs laser and 4 times higher than that of picosecond (ps) laser. Further increasing of the throughput is expected by using higher repetition and higher scanning speed. This technology offers the great potential in applications such as constructing sensitive detectors and sensors, solar energy absorber, and biomedicine. © 2015 Optical Society of America

OCIS codes: (060.3510) Lasers, fiber; (140.3390) Laser materials processing; (220.4000) Microstructure fabrication; (220.4241) Nanostructure fabrication.

<http://dx.doi.org/10.1364/AO.54.000324>

1. Introduction

Recently, femtosecond (fs) laser direct writing has become an advanced tool for high-quality material microprocessing and nanoprocessing, more controllable with minimal thermal damage to surrounding materials. Among these, laser surface modification has been increasingly investigated to synthetically alter surface properties, such as optical properties [1–10], wettability [11–15], and biological properties [16–19]. Blackening and coloring of metal and non-metal surfaces are important to both military and commercial applications, such as camouflage, optical sensing and imaging, countermeasure, solar cell, engraving, marking, etc.

Researchers have already made advances in this fs laser blackening field by using solid-state Ti:sapphire fs lasers. For example, Mazur and co-workers [1,2] conducted the pioneering work of fs laser-induced microstructuring on silicon surface and improved its optoelectron conversion efficiency. Vorobyev and Guo [4,6] developed a technique to transform highly reflective metals to be either totally absorptive or reflecting only a certain color of light, creating so-called black or colored metals by using fs laser direct writing. However, the blackening by using solid-state fs laser is quite time consuming, the processing speed is usually in the magnitude of micrometers per second. The speed is mainly limited by the low pulse repetition rate (kHz) of Ti:sapphire fs lasers. Moreover, solid-state fs lasers are bulky, expensive, and not user friendly.

Researchers have tried to increase the processing speed by using different methods, such as the

1559-128X/15/020324-10\$15.00/0
© 2015 Optical Society of America

interferometric method [20,21] or a nanosecond (ns) laser [22], but the high throughput was compromised by reduced blackness. Furthermore, the ns laser could cause heat buildup, resulting in product distortion and progressive variation in color. Recently, higher processing throughput was obtained by using a picosecond (ps) laser for copper blackening [23], but it is still not enough for industrial applications. Recent advances in laser technology have evolved more compact and reliable high-power and high repetition rate fs fiber lasers for many industrial applications.

In this paper, super-blackening of metals using a high-power and high repetition rate fs fiber laser is studied. The fs laser blackening mechanisms are discussed. Different laser writing conditions, including pulse energy, repetition rate, writing speed, and pitch, are investigated for the blackening effect. Different surface morphologies are generated and characterized using optical microscopy and scanning electron microscopy (SEM). The wavelength dependence of the reflectance of electromagnetic irradiations in the UV, visible, near-infrared (NIR), middle-wave infrared (MWIR), and long-wave infrared (LWIR) regions is characterized and measured. For specific wavelength the reflectance can be less than 1%. In addition to the high broadband absorption, this process can also make the surfaces hydrophobic or hydrophilic simultaneously. Furthermore, the fs fiber laser based method enables the processing speed up to hundreds of millimeters per second, much higher than those reported with other lasers. This novelty makes the high-power and high repetition rate fs fiber laser an efficient and affordable method for practical industrial applications.

2. Experimental Setup and Materials

For the experimental setup, it comprises a mode-locked fiber laser system, beam delivery components, an acousto-optic modulator (AOM), an automated motion system, a sample fixture, and a computer for system control. The fs fiber laser system was a commercialized high-energy fiber laser (Uranus Series, PolarOnyx Laser, Inc.), generating 750 fs pulses (FWHM) at 1030 nm wavelength with pulse repetition rate from 50 kHz up to 1 MHz. In the experiments, the laser beam was guided by mirrors toward to a scanner (ScanCube 10, SCANLAB AG) and focused by an F-theta lens ($f = 100$ mm) onto the sample. The sample was mounted on a computer-controlled five-dimensional translation stage. The pulse energy was adjustable by the AOM. The output collimated beam was a nearly symmetric Gaussian with $M^2 < 1.3$ and the maximum output pulse energy was 500 μ J. An attenuator was used to control the laser pulse energy. The total beam delivery loss was less than 20%. A CCD camera was used to obtain a live view for the laser direct writing. All experiments were carried out in ambient air. Before and after the laser processing, the samples were cleaned by an ultrasonic cleaner. The focal spot size for the

laser beam was 25 μ m ($1/e^2$). A constant air flow was placed across the sample surface during the experiment to flush out the plume of ablated and recondensed material.

In this study, different types of metals were used for laser direct writing, including aluminum, copper, titanium, and stainless steel. Samples were prepolished and carefully cleaned before each experiment. After the laser processing and polishing, the laser written structures were captured and characterized by optical transmission microscopy (ME520T-9M). Then a SEM (FEI QUANTA FEG 600) with energy-dispersive x-ray spectroscopy (EDS) detector was used to further characterize and measure the features.

The wavelength dependence of the total reflectance was characterized with different spectrophotometers for different wavelength ranges. The reflectance for visible wavelength (360–740 nm) was measured by using a visible wavelength spectrophotometer (CM-2600d, Konica Minolta), and it provides both $L * a * b$ values (CIE Lab color space) and total reflectance values. To explore the reflectance in the NIR, MWIR and LWIR region, a NIR spectrophotometer (200 nm–2.5 μ m, LAMBDA 1050 UV/Vis/NIR, Perkin Elmer) and a FT-IR spectrometer (2.5–15 μ m, Frontier FT-NIR/MIR, Perkin Elmer) were used. For the total reflectance measurement, an integrating sphere with 150 mm diameter was used to measure both the specular and diffuse reflections of the processed surface.

3. Experimental Results and Discussion

To systematically study the blackening effect using an fs fiber laser, different laser parameters and processing conditions were evaluated for different metals. A series of experiments were carried out to investigate the correlation of blackening quality with laser pulse energy, repetition rate, pitch, and scanning speed.

A. Mechanism and Process Optimization

1. Aluminum Blackening

Aluminum blackening was conducted with various conditions, including scanning speed (0.001–1 m/s), pulse energy (2.8–13.5 μ J), and scanning pitch (5–50 μ m). The pulse repetition rate was fixed at 100 kHz. For each parameter set, the sample was scanned in both horizontal and vertical directions. The scanning pitch (5–50 μ m) covers from smaller to larger than focal spot size.

Several kinds of surface colors (Fig. 1) can be generated on the aluminum surfaces by varying the

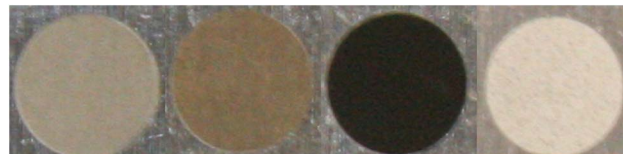


Fig. 1. Photographs of modified aluminum surface showing different colors: (a) gray; (b) golden; (c) black; and (d) white.

scanning conditions. It is believed that the surface colors of the modified area are mainly related to the surface morphology [3–6,22,23]. Given the same pulse energy and pitch, as the scanning speed decreases from 500 to 2 mm/s, the color goes from light gray, gold, black, to white. For the same pulse energy and scanning speed, the color becomes darker with the decreasing scanning pitch.

Figure 2(a) shows the measured total reflectance of the aluminum sample as a function of wavelength for different scanning pitches. The fs fiber laser processing with proper parameters significantly decreases the reflectance of the aluminum surfaces in a broadband spectrum. Strong light absorption was achieved after processing on initially high-reflective polished aluminum surfaces. The scanning pitch between two adjacent lines has obvious influence on the reflectance when using the same pulse energy (13.5 μJ) and scanning speed (10 mm/s). As the scanning pitch increases from 5 to 50 μm , the total reflectance increases. For each scanning pitch, the reflectance increases with the wavelength. The lowest reflectance was obtained with a scanning interval of 5 μm , with over 95% absorptivity in the visible spectral region and 97% absorptivity at some specific wavelength(s).

Figure 2(b) shows the reflectance as a function of wavelength with different scanning speeds. Other scanning conditions are kept the same—13.5 μJ pulse energy and 10 μm scanning pitch. At low scanning speeds (e.g., 50 mm/s), the reflectance for the whole wavelength range is almost uniform and the total reflectance is less than 2%. At 100 mm/s scanning speed, the reflectance increases with the wavelength but the total reflectance is still less than 5%. At even higher scanning speeds (200 and 300 mm/s), the wavelength-dependent reflectance increases more dramatically and the total reflectance is about 6% and 9%, respectively. It is worth to mention that with further decreases of the scanning speed to 5 or 2 mm/s, the reflectance suddenly increases and the aluminum surface becomes white rather than black color (Fig. 1).

To understand the mechanism that causes these optical properties of fs fiber laser processed aluminum surfaces, a detailed study of the surface structure was performed. Figure 3 shows the SEM view of surface structures created with different scanning pitches. With the increase of scanning pitch, different kinds of microstructures can be introduced onto the sample surfaces. When the scanning pitch is smaller than the focal spot diameter [Figs. 3(a) and 3(b)], the entire surface was processed and modified by more overlap of laser pulses, some coral-like surface structures composed of microcavities were produced and these structures seem self-assembled with random orientations. These microcavities consist of small holes in the micrometer range, forming a kind of porous structure. Furthermore, the holes for smaller pitches [5 μm , Fig. 3(a)] are denser and deeper than larger pitches [10 μm , Fig. 3(b)]. When the scanning pitch (30 μm) is equivalent to the focal spot diameter, regularly distributed surface structures begin to show up. The microcavities consisting of larger holes in the 10–20 μm range are fabricated [Fig. 3(c)]. When the scanning pitch (50 μm) is larger than the focal spot diameter, only a certain portion of the surface can be irradiated directly by laser pulses, and trenches crossing each other are created [Fig. 3(d)].

Figure 4 shows the SEM view of surface structures created with different scanning speeds as in Fig. 2(b). When the scanning speed is higher than 300 mm/s for the fixed pulse energy and scanning pitch, no microcavities are formed, only microscale/nanoscale particles can be seen and the modified sample surface looks gray. At 200 mm/s scanning speed, a small amount of microcavities can be seen but the hole is very shallow. The modified surface looks golden, as shown in Fig. 1. When the scanning speed decreases to 100 or 50 mm/s, the porous structure and microcavities become more noticeable and the holes are distributed densely and deeply. This is especially true for 50 mm/s scanning speed. When further decreasing the scanning speed to 5 mm/s, the porous

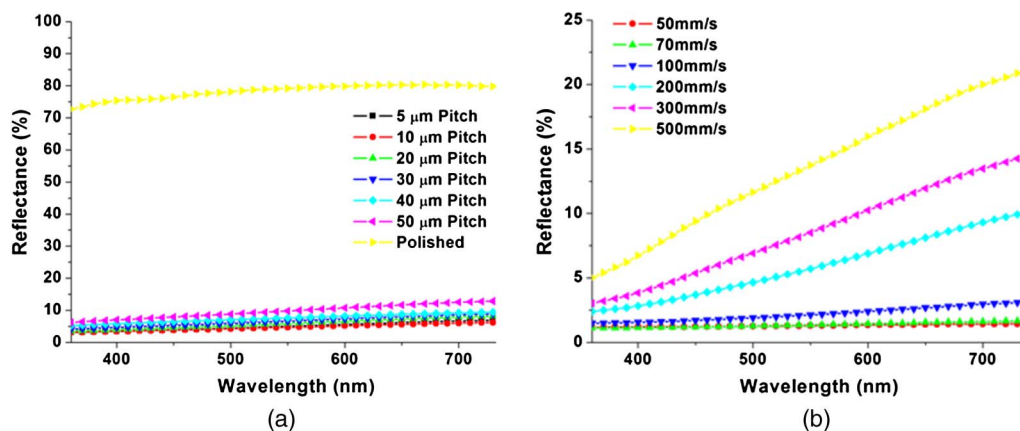


Fig. 2. (a) Reflectance as a function of wavelength for aluminum samples with different scanning pitches. For comparison, the reflectance of polished aluminum surface is also plotted. (b) Reflectance as a function of wavelength for aluminum samples with different scanning speeds.

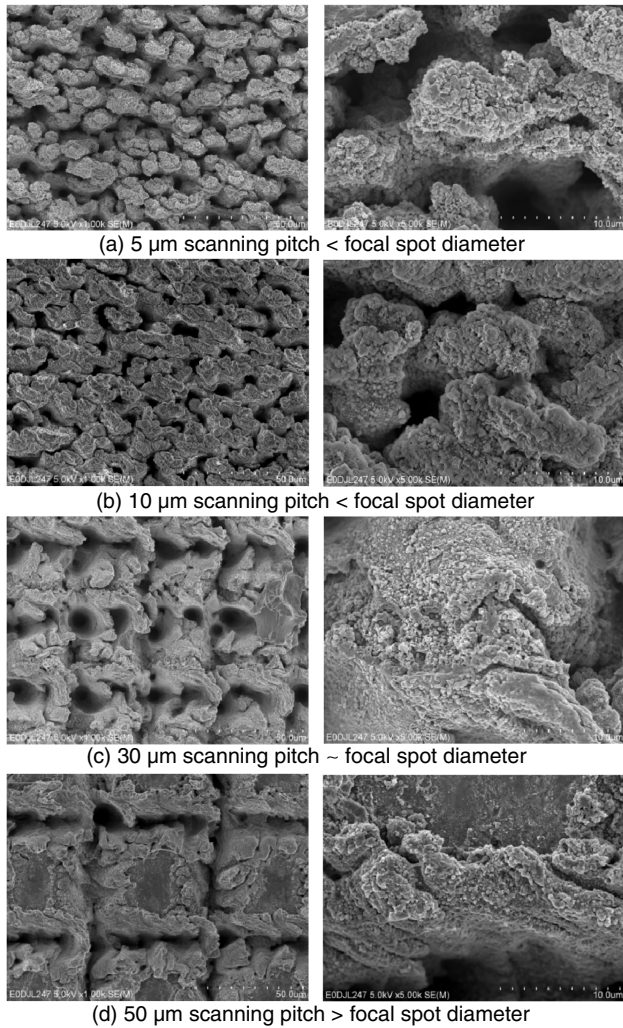


Fig. 3. SEM view of aluminum surface structures after fs fiber laser processing with different scanning pitches: (a) 5 μm pitch; (b) 10 μm pitch; (c) 30 μm pitch; and (d) 50 μm pitch. Right side is the magnified view for the left picture on the same row.

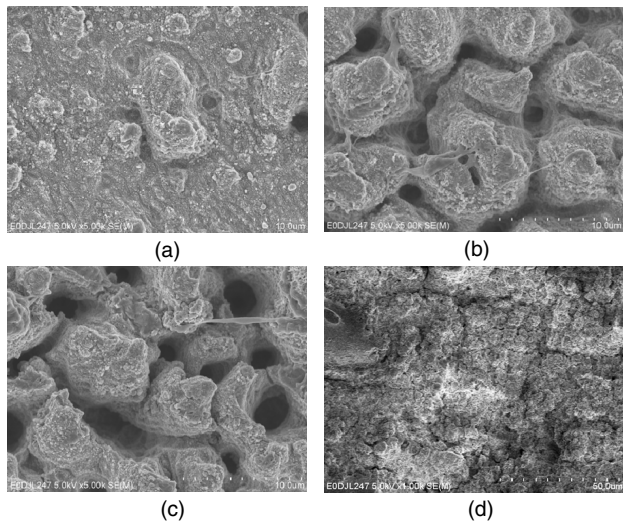


Fig. 4. SEM view of aluminum surface structures after laser processing with different scanning speeds: (a) 300 mm/s, (b) 100 mm/s, (c) 50 mm/s, (d) 5 mm/s.

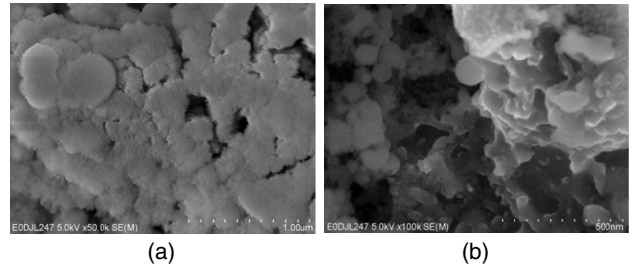


Fig. 5. SEM view of aluminum surface structures with nanostructure and nanoparticles covering the surface: (a) 10 μm pitch and 10 mm/s; (b) 10 μm pitch and 50 mm/s.

structure and microcavities are damaged and disappear due to too much pulse overlapping, and the processed sample surface shows white color in Fig. 1. Figure 5 shows the SEM view of nanostructure and nanoparticles covering the surface of microprotrusions as shown in Figs. 3 and 4. It is well recognized that the composition change of the sample surface was confirmed not to be the main reason for the dramatically enhanced absorption by other researchers and the enhanced broadband absorbance has been demonstrated to result from formation of irregularly distributed surface microspikes and microparticles/nanoparticles [22,23]. In this study, it is believed that light trapping plays a significant role in the processed metal surface to absorb light from a wide angle of view. Figure 6 illustrates such a progressive absorption improvement with various types of structures. The 2D contour patterning process plays a critical role to obtain angular-insensitive surface absorber. For the porous structure shown in Figs. 3 and 4, the randomly distributed large hollow and small hole embedding architecture can effectively collect the incident light in a broad spectrum from all directions. The microstructures and nanostructures and particles on the wall of the holes strengthen the light trapping by blocking the collected light from escaping the cavities. It has also been reported that this porous coral-like structure can act as black holes or light traps to seize the external irradiations effectively, and subsequent multi-reflections inside these blind holes will help convert

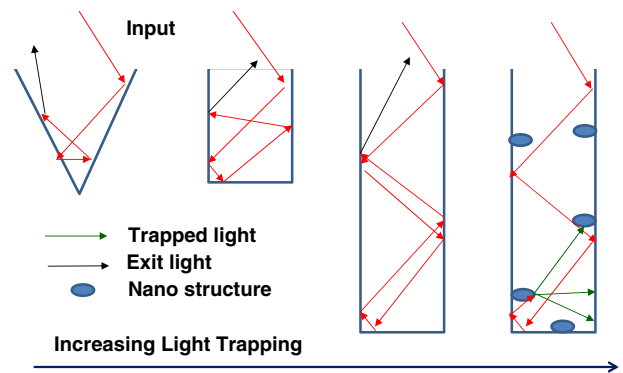


Fig. 6. Illustration of light trapping improvement with high aspect ratio microholes with nanostructures.

the light energy into the heat through iterative absorption [5].

The blackening effect shows a strong relationship with the spatial overlapping of laser pulses. As shown in Fig. 2, good results were obtained when smaller scanning pitch (e.g., 5–10 μm) or slower scanning speed (e.g., 10–50 mm/s) was used. During pulse laser treatment, two factors influence the blackening results, namely pulse energy and pulse overlap rate (total pulse numbers for one spot). The pulse overlap rate is defined by scanning speed, scanning pitch, and pulse repetition rate. At the fixed repetition rate, a smaller pitch or slower speed creates more pulse overlapping and accordingly more laser energy irradiated at one spot. So it was anticipated that 250–1250 pulses per spot was a proper range for the enhancement of absorptance under the highest pulse energy utilized in this study; higher pulse overlapping on the sample surface will damage the surface structure created by previous pulses and a white color surface would be obtained.

2. Copper Blackening

Figure 7(a) shows the reflectance as a function of wavelength for copper samples with different scanning pitches. The other processing parameters are the same: 13.5 μJ pulse energy and 20 mm/s scanning speed. For each scanning pitch, unlike the aluminum sample, the reflectance is almost constant for wavelength below 600 nm and starts to increase for longer wavelength. The total reflectance increases with the increase of the scanning pitch from 5 to 50 μm . The lowest reflectance was obtained with a scanning interval of 5 μm , with over 98% absorptivity in the visible spectral region.

Figure 7(b) shows the reflectance as a function of wavelength with different scanning speeds. The other scanning conditions are the same: 13.5 μJ pulse energy and 5 μm scanning pitch. For all four different scanning speeds, the wavelength-dependent reflectance increases with the wavelength and the increasing rate is faster for wavelength above 550 nm.

A higher scanning speed has faster increasing rate than lower scanning speeds.

Figure 8 shows the SEM view of surface structures created with different scanning pitches at the same scanning speed (10 mm/s). Similarly, different kinds of microstructures can be introduced onto the sample surfaces with the scanning pitch ranging from smaller to greater than the focal spot diameter. With the scanning interval being much smaller than the focal spot diameter, the entire area was processed with pulse overlap rate (i.e., repetition rate/scanning speed) around 625 pulses per spot, coral-like surface structures with microcavities were produced. These structures seem self-assembled with random orientations [Fig. 8(a)]. The microcavities consist of small holes with dimensions of 1–10 μm , forming a porous structure. When the scanning pitch was close to the focal spot diameter, bell mouth-like structures were fabricated [Fig. 8(b)]. When the scanning pitch was larger than the focal spot diameter, only a certain portion of the surface was irradiated directly by the laser focus spot, and shallow trenches were created crossing each other and microparticles and nanoparticles were seen in the trenches [Fig. 8(c)]. Meanwhile, it is found that unlike aluminum sample, the porous structure on the copper surface looks more like explosion where microparticles and nanoparticles are randomly distributed on each exploded surface and inside the hole, whereas the porous structure in aluminum surfaces looks like etching and the small particles are also randomly distributed on each surface and inside the hole.

Furthermore, the processing efficiency and performance in this study was also compared with the experimental results using other types of lasers, such as ps [23] laser and solid-state fs laser [6]. It is inspiring to see that to achieve the total reflectance close to other lasers for the visible spectral range, the processing efficiency in this study is at least 8 times higher than the fs laser source and twice as high as the ps laser sources. The solid-state fs laser processing can blacken the aluminum surface with an area

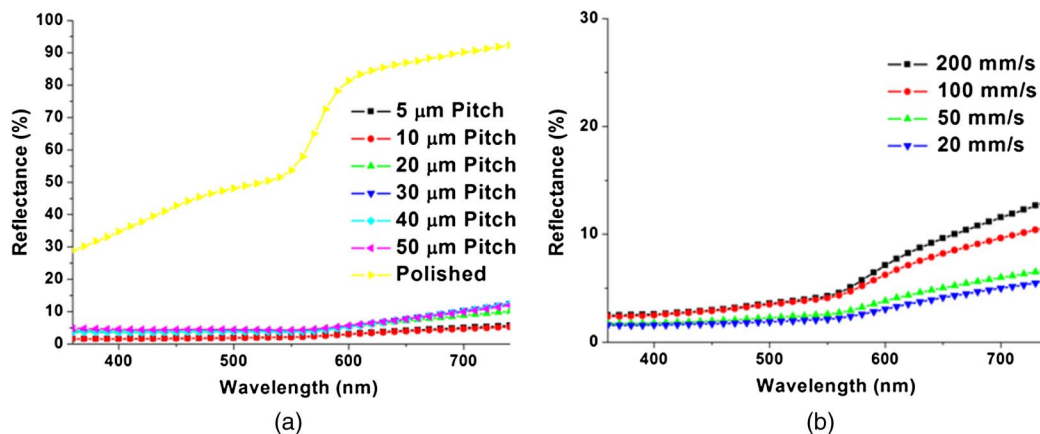


Fig. 7. (a) Reflectance as a function of wavelength for copper samples with different scanning pitches. For comparison, the reflectance of polished copper surface is also plotted. (b) Reflectance as a function of wavelength for copper samples with different scanning speeds.

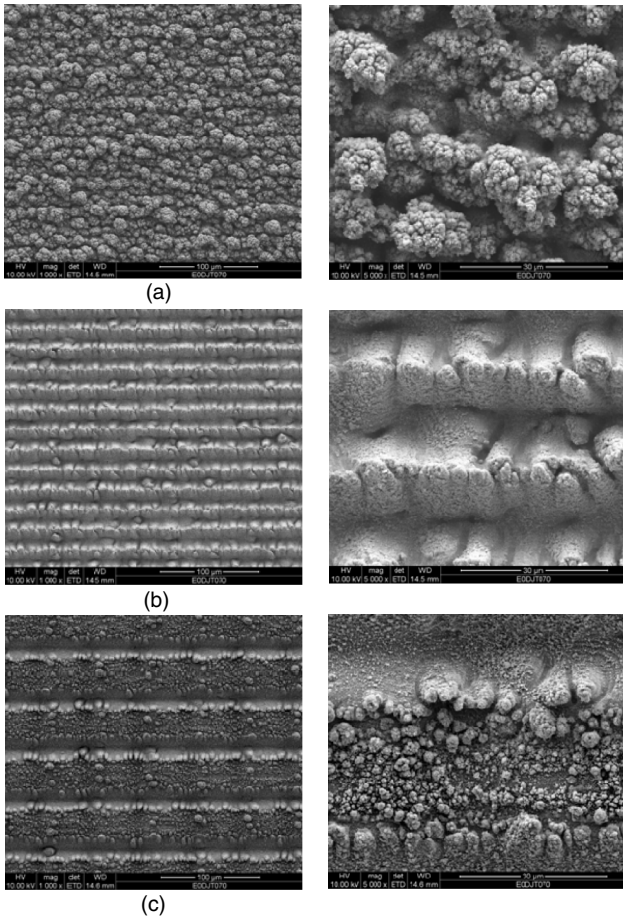


Fig. 8. SEM view of copper surface structures after laser processing with different scanning pitches: (a) 10 μm pitch; (b) 20 μm pitch; and (c) 50 μm pitch. Right side is the magnified view for the left picture on the same row.

of 360 mm^2 within an hour, and for ps laser, a copper surface of 900 mm^2 can be blackened within an hour. In this study, the processing time is within 15 min for a surface of 900 mm^2 (100 mm/s and 10 μm pitch). The repetition rate in our study is only a half of the ps laser. With the further increase of the pulse energy and the repetition rate to MHz level, for

the fs fiber laser, it is believed that the processing speed can be enhanced to hundreds of millimeters per second. This makes the high repetition rate fs fiber laser an efficient and affordable tool for practical industrial applications. Moreover, multibeam can be created by diffractive optical element to further increase the volume fabrication capability by multiple folds at a low cost (by sharing a single laser).

3. Pulse Repetition Rate Impact on Blackening

The pulse repetition rate in relation to scanning speed is also critical to the performance of the blackening process. Figure 9 shows the measured lightness (L) values representing lightness in CIE Lab color space for different speeds (50–500 mm/s) and repetition rates (50–500 kHz) with 5 μm pitch for stainless steel. Lower values of lightness indicate more darkness.

At a fixed repetition rate, L value increases with the scanning speed [Fig. 9(a)]. For low repetition rate (50, 100, and 200 kHz), the increase of L value is more dramatic at slower scanning speed (<200 mm/s) than higher scanning speed (>200 mm/s). For high repetition rate (350 and 500 kHz), the L value increases with the increase of scanning speed from 20 to 100 mm/s, and tends to plateau from 100 to 300 mm/s.

Figure 9(b) shows the L value as a function of repetition rate with different speeds (50–500 kHz, 5 μm pitch, single direction). For each case, the number of pulses fired per spot for each case can be approximately calculated from the repetition rate, the focal spot size, the scanning pitch and the speed [23]. For example, for the case of 50 kHz, the number of pulses for different speeds (50 mm/s, 100 mm/s, 200 mm/s, 300 mm/s, and 500 mm/s) can be calculated as 125, 62, 31, 20, and 12; for the case of 100 kHz, the number of pulses for different speeds (50 mm/s, 100 mm/s, 200 mm/s, 300 mm/s, and 500 mm/s) can be calculated as 250, 125, 62, 41, and 25. For slower scanning speeds (50 and 100 mm/s), the L value decreases at low repetition rate (from 50 to 100 kHz), and then increases at high

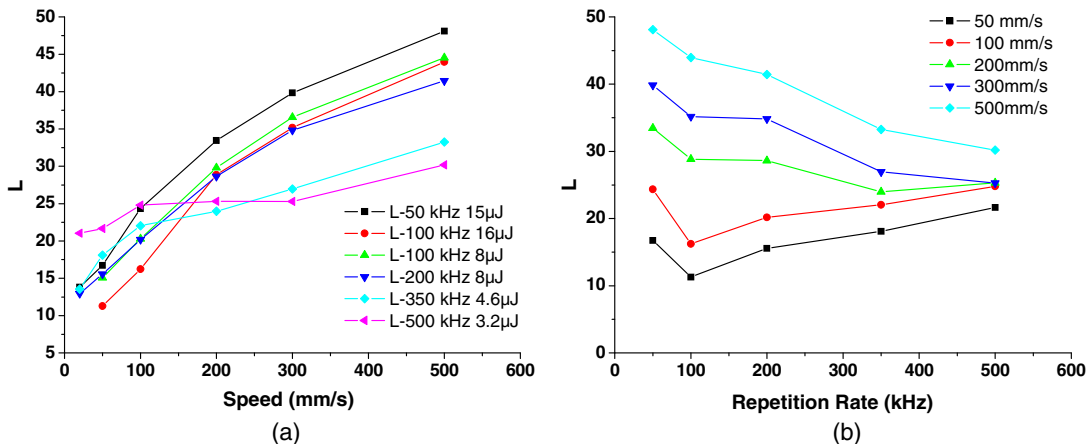


Fig. 9. Lightness measurement for stainless steel with different speeds (a) and repetition rates (b).

repetition rate (from 100 to 500 kHz). For higher scanner speeds (200, 300, and 500 mm/s), the L values decreases when the repetition rate increases from 50 to 500 kHz. The results suggests that high repetition rate favors the reduction of reflectance and combination of high repetition rate and high scanning speed can achieve better reflectance with high throughput.

4. MWIR and LWIR Properties

The blackened samples were measured for the total reflectance from 200 nm to 2.5 μm and the specular reflectance from 2.5 to 15 μm with three different incident angles: 10, 40, and 60 deg. Both the processed sample and polished (unprocessed) sample were measured for comparison. Figures 10 and 11 show the results for different metal types. The processing laser parameters are also provided.

Figure 10 shows the total reflectance for stainless steel blackening. The total reflectance increases from 1.5% to about 5.5% when the wavelength increases from 200 nm to 2.5 μm . When the wavelength changes from 2.5 to 15 μm , the specular reflectance increases from 0.12% to 3.68% for 10 deg incident

angle, from 0.14% to 2.87% for 40 deg incident angle, and from 0.71% to 7.34% for 60 deg incident angle.

Figure 11 shows the reflectance for a titanium sample after blackening. When the wavelength changes from 200 nm to 2.5 μm , the total reflectance increases from 1.0% to 3.0%. When the wavelength changes from 2.5 to 15 μm , the specular reflectance increases from 0.63% to 1.28% for 10 deg incident angle, from 0.93% to 3.15% for 40 deg incident angle, and from 2.29% to 9.63% for 60 deg incident angle.

B. Other Properties of the Blackened Surface

1. Superhydrophobic and Superhydrophilic Property

The control over wetting properties of the material surface has various applications in the chemical, biological, and medical sciences as well as in our everyday life. In this study, both superhydrophobic and superhydrophilic surfaces have been achieved simultaneously with the blackening on different metals, including stainless steel, aluminum, and titanium. When the water drops on the superhydrophilic surface, it is immediately absorbed and spread without any sitting moment. In contrast, when the water drops on the superhydrophobic surface, the water

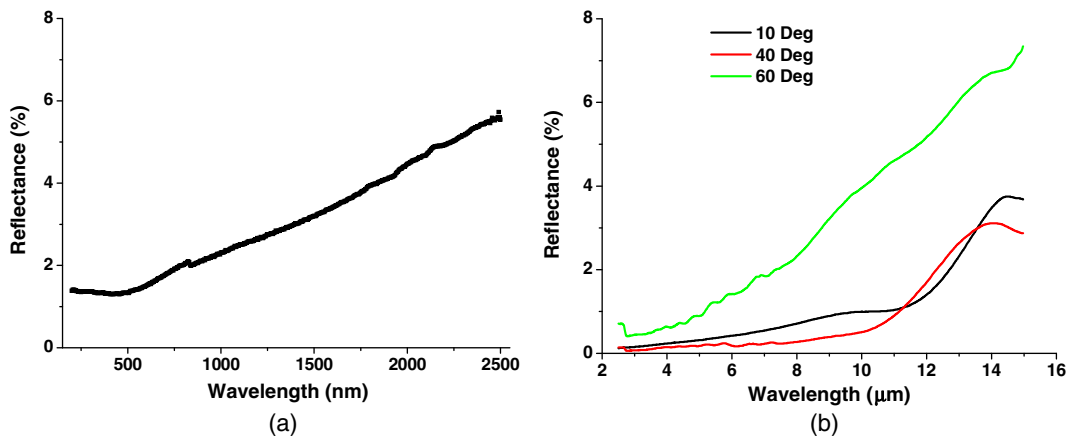


Fig. 10. Reflectance for stainless steel blackening: (a) total reflectance from 350 nm to 2.5 μm ; (b) specular reflectance from 2.5 to 15 μm .

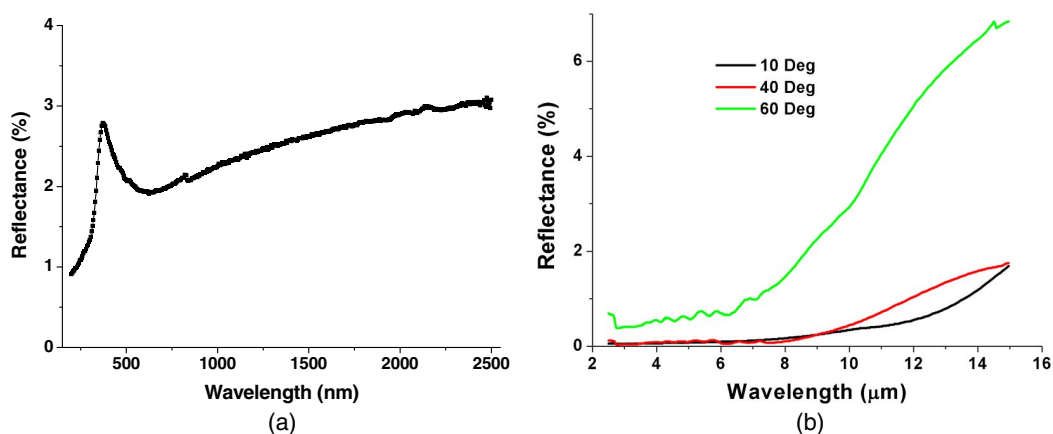


Fig. 11. Reflectance for titanium blackening: (a) total reflectance from 350 nm to 2.5 μm ; (b) specular reflectance from 2.5 to 15 μm .

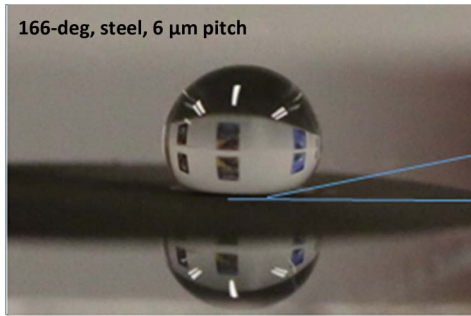


Fig. 12. Camera view of superhydrophobic contact angle of processed stainless steel sample.

bounced off. We have achieved superhydrophobic property in all of the metals with contact angle larger than 166° and roll-off angle less than 3° , as shown in Fig. 12.

2. Thermal Property

The processed metal samples are placed on the top of a hot plate (15×15 cm) to test the thermal transfer properties with a thermal imaging CCD camera (i7, FLIR). The temperature of the plate is set to be around 200°C . Figure 13 shows the thermal images for the hot plate and the cold stainless steel testing sample. The temperature listed in each figure shows the spot temperature measurement results either on an unprocessed or processed sample area. Figure 13 shows temporal development of thermal transfer property for a period of 10 min. The blackened areas have much higher capability of absorbing/trapping heat. At equilibrium they stay at 183°C , while the unblackened areas stay at 65°C . The less blackened area has lower temperature than the blackened area, but its temperature is still higher than the unblackened area.

Figure 14 shows temporal development of thermal transfer property of a titanium sample. The temperature of the titanium sample increases about 2 times compared with stainless steel sample due to its

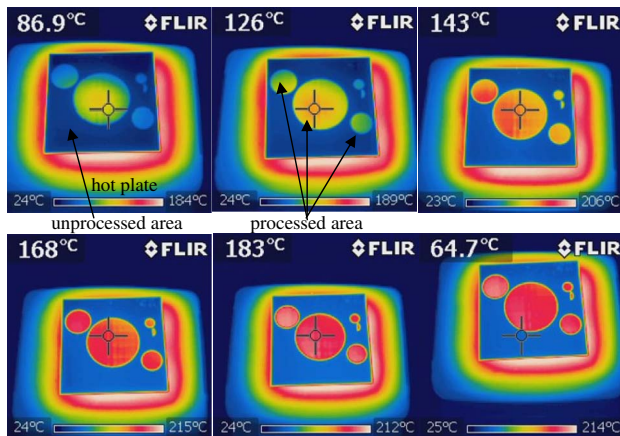


Fig. 13. Temporal dependence of thermal transfer property of stainless steel hydrophilic sample (circled areas are blackened areas): from top left to bottom right 0.5, 1, 2, 3, 4, and 10 min.

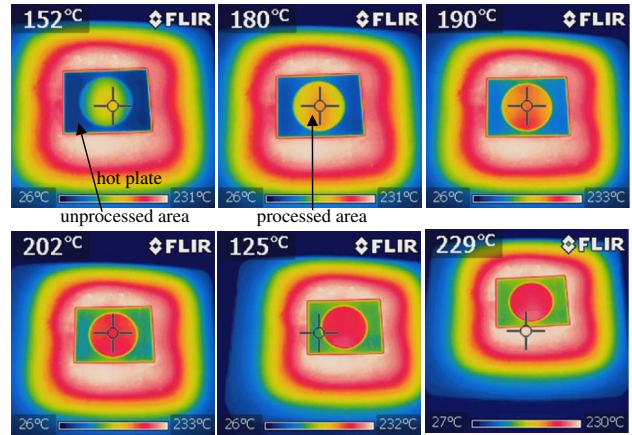


Fig. 14. Temporal dependence of thermal transfer property of titanium hydrophobic sample (circled areas are blackened areas): from top left to bottom right 0.2, 0.5, 1, 2, 3, and 5 min.

higher thermal conductivity. At equilibrium, the blackened areas stay at 202°C , while the unblackened areas stay at 125°C . No difference in thermal transfer properties was observed between hydrophobic and hydrophilic blackened surfaces. Further detailed investigation is needed to make statistical analysis.

C. Cylinder Metal Blackening

Beside metal plates, metal tubes can also be processed and Fig. 15 shows the experimental results of a stainless steel tube inner side blackening. Figure 15(a) shows the camera view of the stainless steel tube inner blackening, while half of the length (left side) is processed and the other half (right side) is unprocessed. The tube has an outer diameter of 25.4 mm and thickness of 1.3 mm.

Figure 15(b) shows the reflection measurement comparison for stainless steel tube inner blackening between processed and unprocessed areas. The processed area has 2%–4% reflection for the wavelength range from 360 to 740 nm, while the original unprocessed area has 25%–35% reflection.

D. Metal Blackening under Anodized Coating

Furthermore, blackening of clear anodized aluminum was also demonstrated, where the blackening is below the anodized layer and the anodized layer was kept intact without damage after laser processing. Figure 16(b) shows the microscopic view of the interface where the left side is the unprocessed area and the right side is the processed area using a fs fiber laser. From the continuity of the texture of the sample on both left and right sides, the top anodized layer is intact and not damaged, where the metal surface below the anodized layer is processed and turned to be black. The reason for the reduced reflectivity is the structuring of the surface under the anodized coating layer.

Figure 16(b) shows the reflectance as a function of wavelength before and after the fs laser processing. The total reflectance drops from 72% to 5% after the

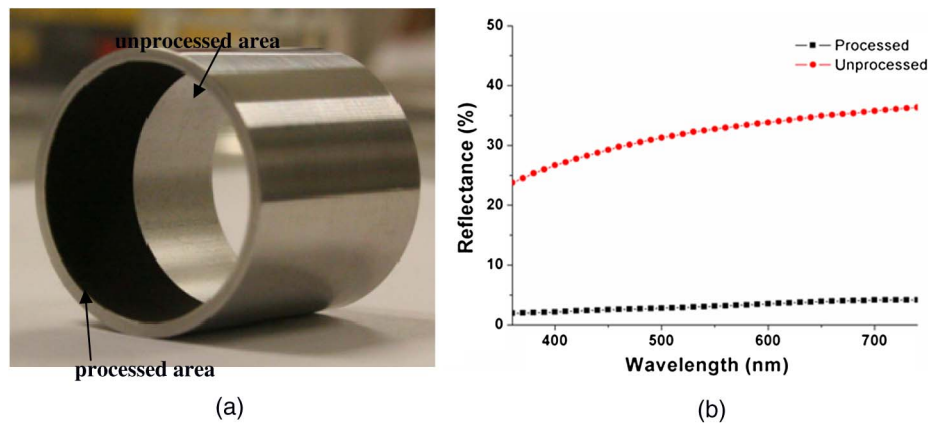


Fig. 15. (a) Camera view of stainless steel tube inner blackening; (b) reflection measurement comparison for stainless steel tube inner blackening between processed and unprocessed area.

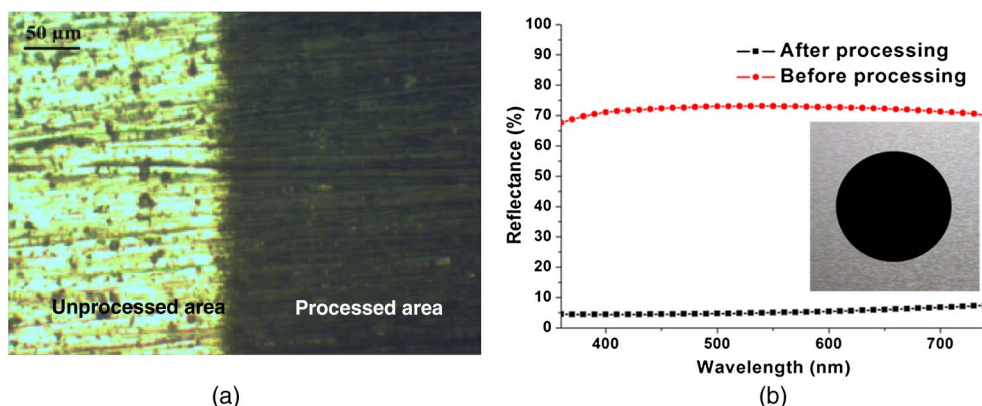


Fig. 16. Clear anodized aluminum blackening using fs fiber laser: (a) Microscopic view of interface between unprocessed area (left) and processed area (right); (b) total reflectance measurement before and after the fs laser processing (insert: a photograph of blackening result with 25 mm diameter).

blackening process. A photograph of the blackened clear anodized aluminum (25 mm diameter) is shown in the middle. The results demonstrate potential applications for metal blackening where the anodize layer or protective layer is needed to be kept intact against harsh environmental conditions.

4. Conclusion

In summary, a high throughput surface microstructuring/nanostructuring technique for super-black and superhydrophobic/hydrophilic surface on both planar and nonplanar metals has been demonstrated. By using a high repetition rate fs fiber laser, light trapping microstructure and nanostructure was generated to absorb light from UV, visible to long-wave infrared spectral region. Different types of surface structures are produced with varying laser scanning conditions. Spectral measurements show that the reflectance of the processed materials decreased sharply in a wide wavelength range and varied at different rates for different scanning pitch and speed. Above 98% absorption over the entire visible wavelength region and above 95% absorption over the NIR, MWIR, and LWIR regions has been

demonstrated. And the absorption for specific wavelengths can go above 99%. Furthermore, the processing efficiency of this fs fiber laser blackening technique is 1 order of magnitude higher than that of a solid-state fs laser and 4 times higher than that of a ps laser with even better absorptivity. Further increasing of the throughput is expected by using higher repetition and higher scanning speed. This study shows the great potential applications, such as constructing sensitive detectors and sensors, solar energy absorber, and biomedicine.

This work was partially supported by DOE, Army, and AFOSR.

References

1. T.-H. Her, R. J. Finlay, C. Wu, S. Deliwala, and E. Mazur, "Microstructuring of silicon with femtosecond laser pulses," *Appl. Phys. Lett.* **73**, 1673–1675 (1998).
2. Z. Huang, J. E. Carey, M. Liu, X. Guo, E. Mazur, and J. C. Campbell, "Microstructured silicon photodetector," *Appl. Phys. Lett.* **89**, 033506 (2006).
3. A. A. Ionin, S. I. Kudryashov, S. V. Makarov, L. V. Seleznev, D. V. Sinitsyn, E. V. Golosov, A. G. Ol'ga, Y. R. Kolobov, and A. E. Ligachev, "Femtosecond laser color marking of metal and semiconductor surfaces," *Appl. Phys. A* **107**, 301–305 (2012).

4. A. Vorobyev and C. Guo, "Femtosecond laser blackening of platinum," *J. Appl. Phys.* **104**, 053516 (2008).
5. Y. Yang, J. Yang, C. Liang, and H. Wang, "Ultra-broadband enhanced absorption of metal surfaces structured by femtosecond laser pulses," *Opt. Express* **16**, 11259–11265 (2008).
6. A. Y. Vorobyev and C. Guo, "Colorizing metals with femtosecond laser pulses," *Appl. Phys. Lett.* **92**, 041914 (2008).
7. B. Dusser, Z. Sagan, H. Soder, N. Faure, J.-P. Colombier, M. Jourlin, and E. Audouard, "Controlled nanostructures formation by ultra fast laser pulses for color marking," *Opt. Express* **18**, 2913–2924 (2010).
8. E. D. Diebold, N. H. Mack, S. K. Doorn, and E. Mazur, "Femtosecond laser-nanostructured substrates for surface-enhanced Raman scattering," *Langmuir* **25**, 1790–1794 (2009).
9. V. V. Iyengar, B. K. Nayak, and M. C. Gupta, "Ultralow reflectance metal surfaces by ultrafast laser texturing," *Appl. Opt.* **49**, 5983–5988 (2010).
10. A. Y. Vorobyev and C. Guo, "Direct femtosecond laser surface nano/microstructuring and its applications," *Laser Photonics Rev.* **7**, 385–407 (2013).
11. T. Baldacchini, J. E. Carey, M. Zhou, and E. Mazur, "Superhydrophobic surfaces prepared by microstructuring of silicon using a femtosecond laser," *Langmuir* **22**, 4917–4919 (2006).
12. V. Zorba, L. Persano, D. Pisignano, A. Athanassiou, E. Stratakis, R. Cingolani, P. Tzanetakis, and C. Fotakis, "Making silicon hydrophobic: wettability control by two-lengthscale simultaneous patterning with femtosecond laser irradiation," *Nanotechnology* **17**, 3234–3238 (2006).
13. P. Bizi-Bandoki, S. Benayoun, S. Valette, B. Beaugiraud, and E. Audouard, "Modifications of roughness and wettability properties of metals induced by femtosecond laser treatment," *Appl. Surf. Sci.* **257**, 5213–5218 (2011).
14. A.-M. Kietzig, M. Negar Mirvakili, S. Kamal, P. Englezos, and S. G. Hatzikiriakos, "Laser-patterned super-hydrophobic pure metallic substrates: cassie to wenzel wetting transitions," *J. Adhes. Sci. Technol.* **25**, 2789–2809 (2011).
15. B. Wu, M. Zhou, J. Li, X. Ye, G. Li, and L. Cai, "Superhydrophobic surfaces fabricated by microstructuring of stainless steel using a femtosecond laser," *Appl. Surf. Sci.* **256**, 61–66 (2009).
16. M. Erdoğan, B. Öktem, H. Kalaycıoğlu, S. Yavaş, P. K. Mukhopadhyay, K. Eken, K. Özgören, Y. Aykaç, U. H. Tazebay, and F. Ö. Ilday, "Texturing of titanium (Ti6Al4V) medical implant surfaces with MHz-repetition-rate femtosecond and picosecond Yb-doped fiber lasers," *Opt. Express* **19**, 10986–10996 (2011).
17. A. Ranella, M. Barberoglou, S. Bakogianni, C. Fotakis, and E. Stratakis, "Tuning cell adhesion by controlling the roughness and wettability of 3D micro/nano silicon structures," *Acta Biomater.* **6**, 2711–2720 (2010).
18. L. He, J. Chen, D. F. Farson, J. J. Lannutti, and S. I. Rokhlin, "Wettability modification of electrospun poly(ϵ -caprolactone) fibers by femtosecond laser irradiation in different gas atmospheres," *Appl. Surf. Sci.* **257**, 3547–3553 (2011).
19. C. Fotakis, V. Zorba, E. Stratakis, A. Athanassiou, P. Tzanetakis, I. Zergioti, D. Papagoglou, K. Sambani, G. Filippidis, and M. Farsari, "Novel aspects of materials processing by ultrafast lasers: From electronic to biological and cultural heritage applications," in *Journal of Physics: Conference Series* (IOP, 2007), pp. 266.
20. J. Kaakkunen, K. Paivasaari, M. Kuittinen, and T. Jaaskelainen, "Morphology studies of the metal surfaces with enhanced absorption fabricated using interferometric femtosecond ablation," *Appl. Phys. A* **94**, 215–220 (2009).
21. K. Paivasaari, J. Kaakkunen, M. Kuittinen, and T. Jaaskelainen, "Enhanced optical absorptance of metals using interferometric femtosecond ablation," *Opt. Express* **15**, 13838–13843 (2007).
22. G. Tang, A. C. Hourd, and A. Abdolvand, "Nanosecond pulsed laser blackening of copper," *Appl. Phys. Lett.* **101**, 231902 (2012).
23. P. Fan, M. Zhong, L. Li, T. Huang, and H. Zhang, "Rapid fabrication of surface micro/nano structures with enhanced broadband absorption on Cu by picosecond laser," *Opt. Express* **21**, 11628–11637 (2013).